ELSEVIER

Journal of Nuclear Materials 276 (2000) 186–193

journal of nuclear materials

www.elsevier.nl/locate/jnucmat

Heavy ion irradiation and annealing of lead: atomistic simulations and experimental validation

M.-J. Caturla*, M. Wall, E. Alonso, T. Díaz de la Rubia, T. Felter, M.J. Fluss

Chemistry and Material Science Directorate, Lawrence Livermore National Laboratory, P.O. Box 808, Livermore, CA 94550, USA

Abstract

We simulated the evolution of the defect microstructure resulting from irradiation of lead with 180 keV Er^+ at liquid Nitrogen temperature followed by an isochronal anneal up to 350 K. The results were validated by comparison with experiments. The simulation consists of a coupled molecular dynamics (MD) and kinetic Monte Carlo (KMC) calculation that follows the production and migration of defects during irradiation and subsequent isochronal annealing. Defect diffusivities and cluster energetics were calculated by MD simulations with and embedded atom-like potential for Pb, or obtained from experiments whenever available. The primary stage of the damage produced by the energetic recoils was also calculated using MD. These calculations show the formation of dense interstitial and vacancy clusters after the cooling of the cascade. The ions are implanted at a temperature of 94 K and the damage is annealed by increasing the temperature on a stepwise fashion by 50 K every 5 min. The time–temperature evolution of the density of point defects and defect clusters is calculated in this simulation. The results are compared with experimental observations for the same irradiation and annealing conditions. The experiments consist of a set of transmission electron microscope (TEM) micrographs taken at different times during the anneal. The micrographs show the presence of loops after irradiation at 94 K, the increase in loop density with temperature, and the disappearance of all the loops at temperatures of ~340 K. These results are in good agreement with the simulations, which help us understand the underlying processes occurring during irradiation and annealing.

1. Introduction

One of the interests in studying microstructure evolution during irradiation is the observed change in mechanical properties of materials exposed to irradiation, such as in the case of materials for fission and fusion reactors. These macroscopic changes are related to the microscopic defects produced during the irradiation. The study of the production and evolution of these defects is fundamental to understand the final macroscopic changes in the material.

During the last decade molecular dynamics (MD) simulations helped understand the nature of the damage produced by self-irradiation of metals during the initial collision cascade ($\sim 10^{-11}$ s) [1]. In particular, these simulations showed that ion irradiation produces a clear separation between vacancies and interstitials, with a rich vacancy core in the damaged area and surrounding self-interstitial atoms. This is a very different picture from the vacancy–interstitial pair production (Frenkel pairs) obtained when multiple collisions are not included in the simulation, like in the case of binary collision models. Cascades produced by different energy ranges have been obtained by MD both in fcc and bcc metals [2–4]. These simulations also showed that clustering of defects can occur during the cooling of the cascade.

The production of vacancy loops as a result of cascade collapse has also been observed experimentally using transmission electron microscopy (TEM) in fcc metals under heavy ion irradiation at room temperature [5]. TEM is a powerful technique commonly used to investigate damage evolution during annealing. One of the advantages of this technique is the possibility of looking at defect evolution at different temperatures. It allows for the direct measurement of defect generation,

* Corresponding author.

0022-3115/00/$ - see front matter
PII: S0022-3115(99)00202-0

growth and shrinkage during annealing. One of the major difficulties in these studies, however, is to distinguish the nature of small defect clusters, that is the vacancy or interstitial character of the defect. Moreover, thin films are used in these measurements that can induce some artifacts, such as loop migration to the nearby surfaces [6]. Single defects can also migrate to nearby surfaces that act as sinks for point defects. Understanding the processes occurring at different temperatures is necessary to interpret these experiments.

Modeling microstructure evolution at finite temperatures has been traditionally done using mean field approximations, due to the complexity of the problem that involves macroscopic time and length scales [7,8]. These models, however, can not account for inhomogeneities in damage production that have been observed experimentally, such as void depletion close to grain boundaries [9] or the presence of dislocations decorated by loops [10]. Kinetic Monte Carlo (KMC) models [11,12], however, allow for an atomistic description of damage production and damage evolution at different temperatures. These models have been recently used to study the number of defects escaping recombination in the cascade core by using results from MD simulations [2,11]. However, the input data used in the simulations needs to be validated with experimental observations.

We have used a combination of experimental TEM measurements and computer simulations to study the damage production and annealing in ion-irradiated lead. The simulation model and input data are described in Section 2. The simulation results for 180 keV Er^+ implantation in Pb and annealing up to room temperature are presented in Section 3, followed by the experimental measurements under similar conditions. In Section 5 we discuss the comparison between experiments and simulations.

2. Simulation model

A coupled MD/KMC approach is used to solve the problem of defect production, defect diffusion, cluster growth and cluster dissolution. This model includes single vacancies, vacancy clusters, self-interstitials and self-interstitial clusters. This simulation is equivalent to the solution of the diffusion equations for all the defects in the system in rate theory. The advantages of a KMC simulation, among others, are that each defect can be treated individually, preserving the microstructural information, any cluster size can be followed with this method, and steady state is not a requirement of the simulation model. Disadvantages are related to the large amount of computer power, both CPU and memory, required to carry out the simulations for realistic doses and dose rates. Clearly, however, these disadvantages are ephemeral as computer power has doubled every 18 months for the last 30 yr and will likely continue to do so for at least another 10 yr.

All the defects in the simulation are considered as individual entities, with a particular capture radius, that depends on the number of elements it represents (for example a di-vacancy has a larger capture radius than a single vacancy). This capture radius determines the distance of interaction between two defects, for example, the distance for a vacancy and a self-interstitial to annihilate. The interaction radius between defects has been defined as

$$r = r_{\mathrm{sph}} + \delta, \tag{1}$$

where

$$r_{\mathrm{sph}} = \sqrt[3]{\frac{3N\Omega}{4\pi}}, \tag{2}$$

with Ω the atomic volume and N the number of defects in the cluster. Since the stress field of single-interstitials is larger than the one of single-vacancies, a larger capture radius is considered for interstitials (r_I) interacting with loops (vacancy or interstitial clusters) than for single vacancies (r_V), $r_1 = 1.15 \times r_V$, where r_V is defined in Eq. (1) above. This includes a bias for the interaction of interstitials and vacancies with the microstructure.

All the interactions between defects occur spontaneously as soon as they are in the capture radius (diffusion limited reactions).

Each defect has associated a set of probabilities to undergo a particular event. Events can be jumps or dissolution of a particle from a cluster. The probability for any of these events happening is given by the diffusivity (in the case of jump probability) and the binding energies of the different clusters (in case of cluster dissociation). Defects move by a fixed distance (first nearest neighbors). For the case of defects moving in three dimensions, the direction of the jump is taken at random, since no lattice is present in this simulation. Only for those defects that move in one dimension both the jump distance and the direction ($\langle 1\,1\,0\rangle$) are fixed. The time is updated every step and is the inverse of the sum of the rates of all possible events.

Values for diffusivities and binding energies of clusters are obtained either from experiments or from empirical MD simulations. Table 1 shows the values for the

Table 1
Migration energies (E_{m}) and diffusivity pre-factors (D_0) for single-vacancies (V) and single-interstitials (I) and Interstitial clusters (n = number of defects in cluster) used in the simulations

Species	D_0 (cm^2/s)	E_{m} (eV)
V	10^{-3}	0.45
I	10^{-4}	0.02
I_n $(2 < n < 40)$	10^{-4}	0.1

Table 2
Formation energies (E_f^X) and binding energies (E_b^X) for small vacancy ($X = V$) and interstitial ($X = I$) clusters as obtained from molecular dynamics simulations

Size	E_f^V (eV)	E_b^V (eV)	E_f^I (eV)	E_b^I (eV)
1	0.51	–	1.12	–
2	0.84	0.16	1.86	0.38
3	1.21	0.13	2.44	0.53
4	1.44	0.27	2.88	0.69
5	1.77	0.17	3.49	0.51
6	–	–	3.51	1.1
7	–	–	4.14	0.49
8	–	–	4.20	1.06

migration energies used in the simulations presented in this paper. The migration energy used in the simulation for vacancies is that obtained experimentally [13]. The single interstitial diffusivity was calculated using MD by computing the mean square displacement of all the atoms in the system at different temperatures. One of the greatest controversies in defect evolution in metals is the mobility of interstitial clusters. Perfect loops should easily glide along a $\langle 1\,1\,0\rangle$ direction. However, small cluster sizes are not perfect but faulted loops, according to elasticity theory [14]. Assuming a stacking fault energy for lead of ~ 0.02 J/m^2, and elasticity models [14] the transition between faulted and unfaulted loops for Pb occurs at a cluster size of approximately 47 nm in radius, therefore, it is reasonable to assume that all clusters with radius smaller than 47 nm (equivalent to approximately 6.5×10^4 defects) are faulted loops and therefore sessile. At sizes on the order of the dislocation core (~ 1 nm) elasticity theory can not be extrapolated and MD simulations seem more reliable. In the last few years, MD simulations have shown that interstitial clusters can migrate with a very low activation energy. Osetsky et al. have shown that in Cu, interstitial clusters can glide on a $\langle 1\,1\,0\rangle$ plane with an activation energy of 0.024 eV [15]. In our simulations we have assumed that those interstitial clusters containing more than 5 defects and less than 40 move in a one-dimensional path along the $\langle 1\,1\,0\rangle$ direction with a migration energy of only 0.1 eV. All those clusters containing more than 40 interstitials are considered to be sessile.

We have calculated the binding energies of vacancies and interstitials in Pb using MD and energy minimization. For these simulations we have used the parametrization obtained by Cleri and Rosato for Pb using the tight-binding second-moment approximation (TB-SMA) [16]. This interatomic potential has the same form as the embedded-atom method (EAM) model developed by Daw and Baskes [17]. The binding energy, $E_b^\alpha(n)$, of a defect cluster with n elements can be defined as

$$E_b^\alpha(n) = E_f^\alpha(n-1) + E_f^\alpha(1) - E_f^\alpha(n),$$

where α is either I (interstitial cluster) or V (vacancy cluster). In a KMC simulation the dissociation energy of a defect from a cluster is given by the sum of the binding energy and the migration energy of that defect. We have calculated the binding energies of small clusters of vacancies and interstitials using the formation energies calculated with MD. We calculated formation energies for different arrangements of defects in a cluster: in a sphere, in a plane or in a row. Values reported here are only for the most stable configuration, that is, the lowest energy cluster for all the different configurations considered. It should be pointed out that sampling of all possible configurations is complicated and it is possible that lower energy configurations than those reported here could be found. In Table 2 we present the results for the formation energies and binding energies of small clusters obtained in the calculations. For large vacancy clusters the functional of the binding energy curve has to be such that the binding energy is equivalent to the formation energy of a vacancy. The lowest energy configuration for vacancy clusters of size 4 and 5 are three-dimensional, therefore, we assume vacancy clusters to grow spherically using a dependence of 2/3 for the binding energy versus number of vacancies. The binding energy curve used for vacancy clusters in the simulations shown here is

$$E_b^V(n) = 0.5 - 0.58(n^{2/3} - (n-1)^{2/3}) \text{ eV}.$$

As above the binding energy of small interstitial clusters is obtained from the results of MD simulations and results are shown on Table 2. In this case, the lowest energy configurations for large interstitial clusters seem to be laying on a plane and a 1/2 dependence of the binding energy is considered. The binding energy curve in this case is

$$E_b^I(n) = 1.12 - 1.81(n^{1/2} - (n-1)^{1/2}) \text{ eV}.$$

Cascade production is considered in the KMC simulation as an event whose probability is given by the dose rate of the simulation. The damage distribution produced by the energetic ions is obtained from empirical MD simulations. For this particular simulations we

had to reproduce the damage of 180 keV Er ions on Pb. We used a binary collision model, TRIM [18], to obtain the recoil spectrum of 180 keV Er ions on Pb. Using MD simulations we obtained the damage produced by 5 keV Pb ions on Pb and 30 keV Pb ions on Pb. Fig. 1 shows the results of one particular 5 keV (Fig. 1(a)) and 30 keV (Fig. 1(b)) cascade in Pb. This figure shows the location of the vacancies (light circles) and the self-interstitials (dark circles) at the end of the collision cascade. Due to the low melting point of Pb, the melted area produced in the first few picoseconds of the collision cascade is very large therefore requiring of simulations containing at least one million atoms. Moreover, the total relaxation time for a cascade is also long: ~50 picoseconds (ps) for a 5 keV cascade and ~120 ps for 30 keV cascades. Simulations by Nordlund et al. [19] have shown that the cooling down rate of the cascade increases with the atom mass and the total number of 'hot' atoms, or the maximum number of atoms in the melted core of the cascade, is higher the lower the melting point of the material. The large relaxation times and cascade areas of our simulations are, therefore, consistent with the results of Nordlund et al. These simulations were performed in a CRAY T3E, using 128 processors, with a CPU time of $\sim 10^{-6}$ s per time step and atom.

The results from the MD simulations show a typical behavior of a self-irradiated metal: vacancies are concentrated in the center of the cascade core with surrounding interstitials [1–3]. The main difference between these results and previously published results on other metals is the large clusters of both vacancies and interstitials formed at the higher energies. For the 30 keV case shown in Fig. 1(b), four interstitial clusters were formed with an average number of 149 interstitial per cluster. 97% of all the interstitials produced are in the form of clusters.

In order to reproduce the recoil spectrum of 180 keV Er ions on Pb we distributed 5 and 30 keV cascades along the range of the ions, according to the energy distribution obtained by the binary collision model. A total of 12 and 4 cascades of energies 5, and 30 keV respectively where randomly distributed in a box 40 nm deep and 16 nm wide, to account for the range and the straggling of the implanted ions. The distribution of damage produced by several 180 keV Er ions were constructed in this manner in order to be used in the KMC simulation. No effort was made to take into account possible effects [20,21] associated with the possibility of having displacement cascades at or near the free surface. However, since Pb has a thick native oxide this may be a reasonable approximation. Moreover, the mean projected range of 180 keV Er on Pb is ~40 nm and since most of the damage is produced close to the ion range, we expect most of the large displacement cascades to happen well into the bulk of the material.

3. KMC simulations and results

We simulated the implantation of 180 keV Er on Pb using the input data explained above. The implantation was done at 94 K for a total dose of 5×10^9 ions/cm^2. The thickness of the simulation box was 80 nm, corresponding to the thickness of the TEM specimen in the experiments. In fact, the energy was selected to be 180 keV in order to have all the damage produced by the ions in a sample thin enough to be used in the microscope. Surfaces acted as perfect sinks for both vacancies and interstitials. After irradiation and before annealing free vacancies, vacancies in clusters and interstitials in clusters are present in the simulation. No single-interstitials or interstitial clusters of size smaller than 40 are present (since we selected clusters of less than 40

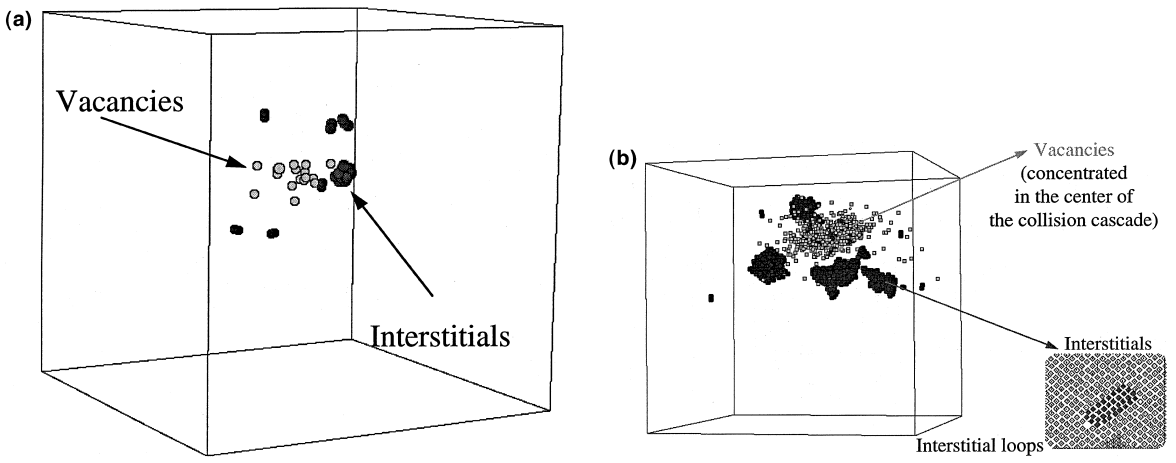

Fig. 1. MD results on self-irradiation of Pb at 5 keV (a) and 30 keV (b).

interstitials as glissile). Due to the low migration energy of these defects, and the one dimensional motion, most of the interstitial clusters recombine with the surfaces during implantation, even at this low temperature. Notice that Stage I in lead, which is believed to be related to interstitial migration, happens at temperatures below 5 K [13]. Most of the vacancies form clusters, with just 27% of all vacancies as isolated defects. This clustering occurs during the cooling down of the cascade and it comes from the MD simulations explained above.

The damage produced by the irradiation is then annealed using a 10 min per step temperature ramp: the temperature is increased by 50 K in 5 min and kept at a constant temperature for another 5 min. Fig. 2 shows the results of the simulation for the total concentration of defects as a function of temperature. Initially most of the vacancies are in clusters (circles), there is a large number of interstitial in clusters (squares) and a few free vacancies (triangles). Between the implantation temperature and 133 K there is no change in defect concentration since all interstitials present are tied up in sessile clusters and vacancies are immobile. At temperatures above 133 K free vacancies start to move (arrow **a** in Fig. 2), corresponding to stage III in Pb (between 150 and 200 K) [13]. The number of free vacancies decreases while the number of vacancies in clusters increases. There is also at these temperatures a slight decrease in the interstitial cluster concentration due to recombination with free mobile vacancies. For temperatures higher than 193 K the total number of vacancies in vacancy clusters decreases due to the dissolution of the smaller vacancy clusters (arrow **b** in Fig. 2), roughly corresponding to stage IV in Pb [13]. Those vacancies coming from the dissolution of small clusters can either recombine with interstitials in clusters, with the surfaces or with other vacancy clusters, therefore, decreasing the total number of vacancies in the system. At the same time those vacancies recombine with the interstitial clusters, resulting in a reduction of the interstitial population. At temperatures between 193 and 300 K the vacancy concentration decreases at a rate of 2.3×10^{15} vacancies/cm^3/K. Notice that stage V, as obtained from resistivity measurements of electron irradiated Pb, occurs at a temperature of ~270 K and higher [13]. However, Schroeder and Schilling already pointed out that recovery processes for lower temperatures could be associated to the dissolution of smaller, less stable clusters, in good agreement with these simulations. At these temperatures, the larger, more stable clusters do not dissolve. For temperatures between 300 and 340 K the rate of disappearance of vacancies is 2.0×10^{16} vacancies/cm^3/K, since at these temperatures even the larger clusters are dissolving. At a temperature of 340 K all vacancy clusters have disappeared from the simulation box and only a few small interstitial clusters are present in the simulation.

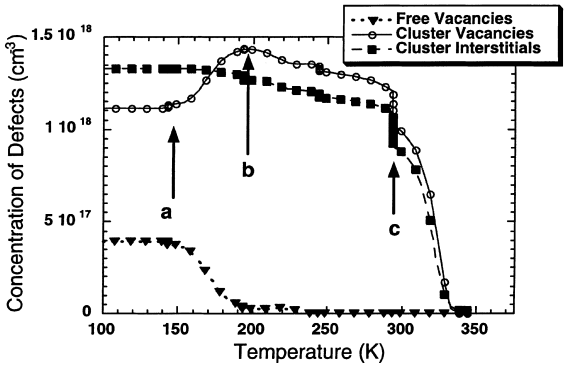

Fig. 2. Total concentration of defects as a function of temperature, during step anneal.

The cluster size evolution for different temperatures is shown in Fig. 3. Between 94 and 200 K the maximum cluster size increases by incorporating free vacancies that are mobile. The small clusters are stable at these temperatures and the vacancy cluster size distribution does not change significantly. Between 193 and 293 K small vacancy clusters start dissociating, and the distribution shifts towards larger sizes, while the cluster concentration decreases, following Ostwald ripening. For temperatures larger than 293 K most of the vacancy clusters dissolve and there is a rapid decrease in defect density. Observe that by 333 K the cluster density is very small. At 340 K all clusters have disappeared. For the case of interstitials, shown in Fig. 3(b), the cluster size distribution moves towards smaller sizes with increasing temperature, since interstitial clusters do not break up at these temperatures, and disappear by dissolution through vacancy–interstitial recombination. The differences between distributions at 94 and 293 K is small, since the number of free vacancies is small. At temperatures higher than 293 K, when large clusters of vacancies break up, the larger super-saturation of vacancies produces larger I–V recombination and the interstitial cluster sizes are greatly reduced, to end up with no interstitial clusters at a temperature of ~340 K.

4. Experiments

TEM samples of high purity Pb were implanted with 180 keV Er ions at low doses ($\sim 5 \times 10^9$ ions/cm^2) at a temperature of 90 K. The sample was then transported to the TEM at the irradiated temperature and annealed in situ. The temperature was raised 50° every 5 min and held for another 5 min before it was raised again. Fig. 4 shows bright field images of the sample at different temperatures during the anneal: (a) as-implanted, (b) 157 K, (c) 213 K, (d) 268 K, (e) 286 K and (f) room

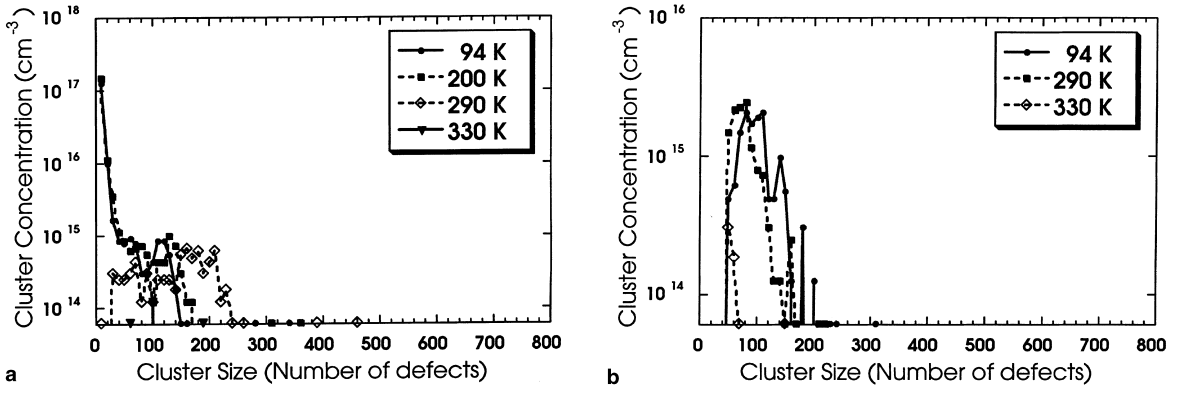

Fig. 3. Clusters size distribution of Vacancies (a) and Interstitials (b) for different temperatures during the step anneal.

temperature after anneal to 340 K. Loop densities were obtained from an area of ~0.4 μm^2. The average diameter of the loops varied from a minimum of 4.7 nm to a maximum of 9.1 nm at different temperatures during the anneal. Fig. 5 shows the loop density as a function of the anneal temperature. Observe that as the temperature increases, so does the loop density. At higher temperatures the loop density decreases and no loops are detectable under the microscope at temperatures of ~340 K.

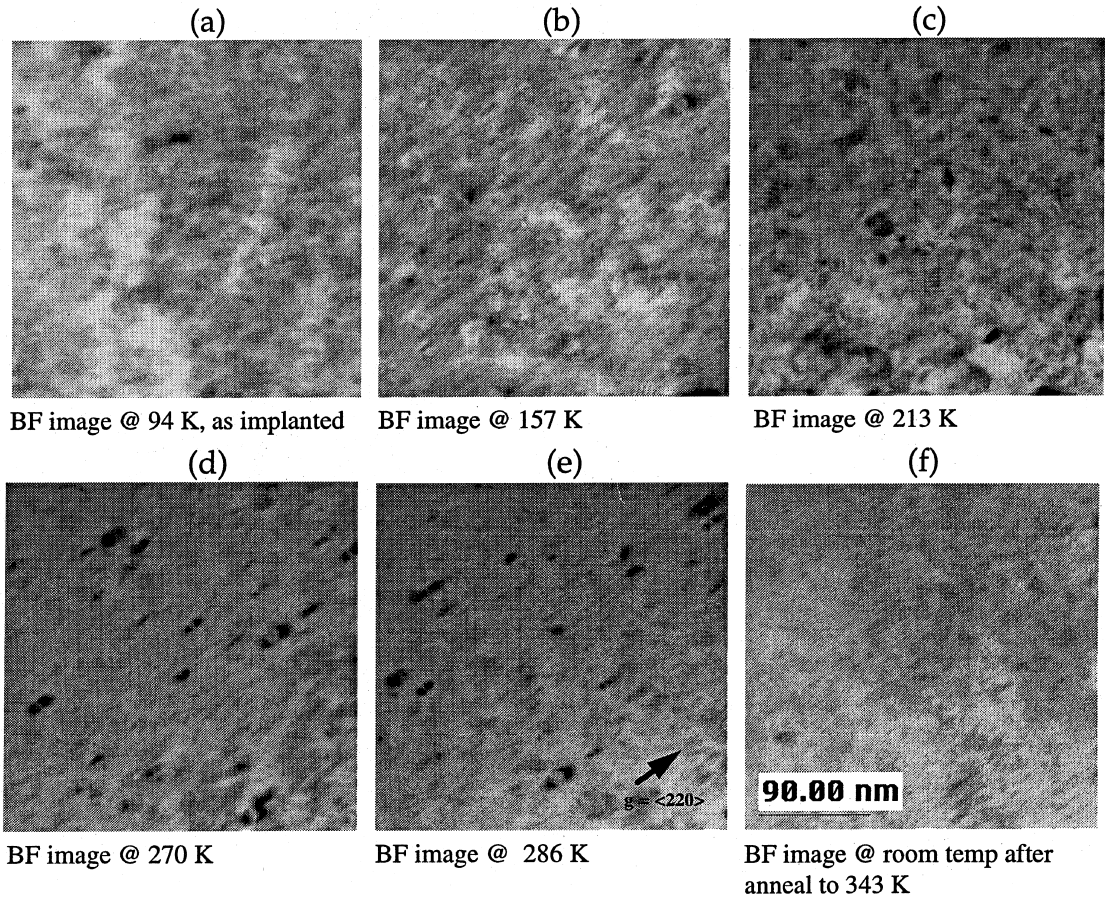

Fig. 4. TEM images during the anneal (a) as-implanted (b).

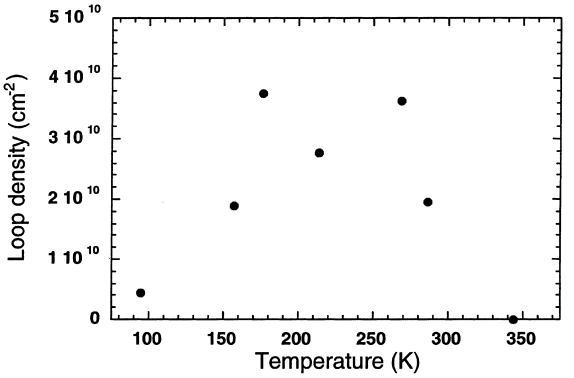

Fig. 5. Density of loops as a function of the annealing temperature as obtained from the experiments.

5. Discussion

In order to compare with the experimental results, we considered only those clusters containing more than 120 defects (interstitials or vacancies) corresponding to loops of radius ~2 nm, assuming that the number of defects (N) in a loop is $N = 4\pi R^2/(3^{1/2}a_0^2)$. Thus, we assume that those clusters with a radius smaller than 2 nm will not be visible under the microscope. The cluster densities for those larger than 120 as a function of annealing temperature are shown in Fig. 6. The density of vacancy clusters (open circles) increases with temperature with a peak at about 290 K, while the interstitial cluster density (squares) decreases for all temperatures. As a result there is a slight increase in the total population of loops up to a temperature of ~290 K. At higher temperatures the cluster density decreases and no clusters, either vacancies or interstitials, are present for temperatures higher than 340 K. This simulation shows good qualitative agreement with the experiments presented above. Better statistics both in the simulations and in the experiments are necessary in order to do a quantitative comparison of the results.

It is interesting to note that all visible interstitial clusters disappear in both the simulation and the experiments, even though the maximum anneal temperature is well below the melting point of Pb. One may expect that proximity of the free surfaces would mean that mobile vacancies would disappear before being able to recombine with interstitial clusters. However, because of the localized nature of defect production in cascades, the mobile vacancies dissolve the sessile interstitial clusters as they try to escape their nascent cascade and never escape to the matrix to become freely migrating defects.

In order to test some of the input data in the simulation we have considered a case where all the defects produced are in the form of Frenkel-pairs. We introduce a homogeneous distribution of vacancy and interstitial pairs with the same total concentration as in the case of cascades obtained from MD and used in the previous calculation. The results for the total concentration of defects as a function of temperature is shown in Fig. 7. As expected, all the vacancies are free after irradiation and start clustering during the anneal. However, the maximum cluster size reached is much smaller than in the case of clusters produced in the cascade. Only maximum sizes of 25 defects per cluster are reached in this case, sizes that would not be visible under the microscope. Moreover, all defects disappeared after only 290 K, contradicting the experimental observations.

In conclusion, we have coupled experiments and simulations to understand microstructure evolution in irradiated Pb. The agreement between experiments and simulations gives us confidence that the model is indeed capable of describing the microscopic nature of damage production and evolution in irradiated metals. We

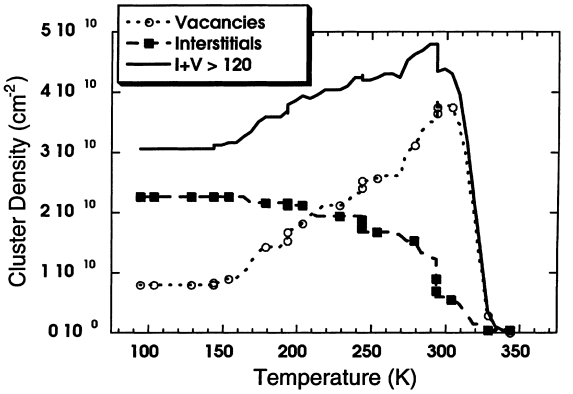

Fig. 6. Density of 'visible' clusters obtained from the KMC simulations. Those clusters containing more than 120 defects are considered visible.

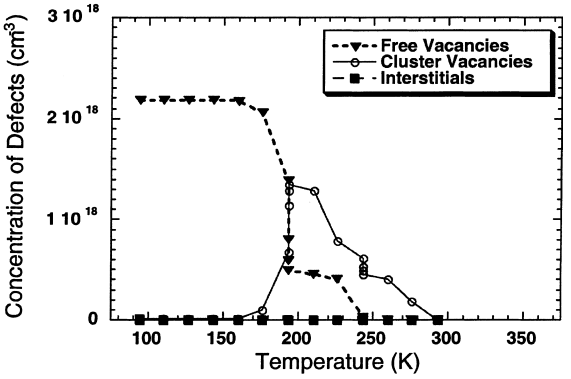

Fig. 7. Total cluster density as a function of annealing temperature obtained from a simulation with starting initial conditions a distribution of Frenkel pairs.

demonstrated that production of defect clusters in the cascade core, followed by the subsequent mobility and clustering/dissolution kinetics of these clusters can explain the experimental observations. A simulation in which the defects where introduced as a homogeneous distribution of Frenkel pairs contradicts the experiments. Further experiments and simulations are on the way in order to develop general, quantitative, and predictive models for radiation damage and defect evolution in metals.

Acknowledgements

This work was performed under the auspices of the US Department of Energy by Lawrence Livermore National Laboratory under contract W-7405-Eng-48.

References

[1] R.S. Averback, T. Diaz de la Rubia, in: Spaepen and Ehrenreich (Eds.), Solid State Physics, vol. 51, Academic Press, New York, 1998, p. 281.
[2] N. Soneda, T. Diaz de la Rubia, Philos. Mag. A 78 (1998) 995.
[3] D. Bacon, J. Nucl. Mater. 251 (1997) 1.
[4] R. Stoller, JOM 48 (1996) 43.
[5] M.L. Jenkins, M.A. Kirk, W.J. Phythian, J. Nucl. Mater. 205 (1993) 16.
[6] M.L. Jenkins, J. Nucl. Mater. 216 (1994) 124.
[7] W.G. Wolfer, J. Nucl. Mater. 122&123 (1984) 367.
[8] L.K. Mansur, J. Nucl. Mater. 216 (1994) 97.
[9] H. Trinkaus, H.B.N. Singh, M. Victoria, J. Nucl. Mater. 233–237 (1996) 1089.
[10] H. Trinkaus, B.N. Singh, A.J.E. Foreman, J. Nucl. Mater. 249 (1997) 91.
[11] H. Heinisch, J. Nucl. Mater. 117 (1983) 46.
[12] G.R. Odette, B.D. Wirth, J. Nucl. Mater. 251 (1997) 157.
[13] H. Schroeder, W. Schilling, Rad. Eff. 30 (1976) 243.
[14] D. Hull, D.J. Bacon, Introduction to Dislocations International Series on Materials Science and Technology, vol. 37, Butterworth–Heinemann, Oxford, 1984.
[15] Y. Osetsky, Mater. Res. Soc. Symp. Proc. 527 (1998) 59.
[16] F. Cleri, V. Rosato, Phys. Rev. B 48 (1993) 22.
[17] M.S. Daw, S.M. Foiles, M.I. Baskes, Mater. Sci. Rep. 9 (1993) 251.
[18] J.F. Ziegler, J.P. Biersack, U. Littmark, in: Stopping and Range of Ions in Solids, vol. 1, Pergamon, New York, 1985.
[19] K. Nordlund, M. Ghalyt, R.S. Averback, M.J. Caturla, T. DiazdelaRubia, J. Tarus, Phys. Rev. B 57 (1998) 7556.
[20] M. Ghaly, R.S. Averback, Mater. Sci. Forum 248&249 (1997) 13.
[21] K. Nordlund, J. Keinonen, M. Ghaly, R.S. Averback, Nucl. Instrum. and Meth. B 148 (1999) 74.